Spectrochimica Acta Part A: Molecular and Biomolecular Spectroscopy 238 (2020) 118430

Contents lists available at ScienceDirect

Spectrochimica Acta Part A: Molecular and Biomolecular Spectroscopy

journal homepage: www.elsevier.com/locate/saa

Damping resonance and refractive index effect on the layer-by-layer sputtering of Ag and Al_2O_3 on the polystyrene template

Daxin Zhang [a,b], Shuo Yang [a,b], Xin-Yuan Zhang [a,b], Ning Ma [c], Bingbing Han [c], Wenshi Zhao [a,b], Shaohua Chi [a,b], Yang Liu [c], Jinghai Yang [c,*], Lei Chen [c,*]

[a] Changchun Institute of Optics, Fine Mechanics and Physics, Chinese Academy of Sciences, Changchun 130033, PR China
[b] University of Chinese Academy of Sciences, Beijing 100049, PR China
[c] Key Laboratory of Functional Materials Physics and Chemistry of the Ministry of Education, Jilin Normal University, Changchun 130103, PR China

ARTICLE INFO

Article history:
Received 3 February 2020
Received in revised form 22 April 2020
Accepted 27 April 2020
Available online 1 May 2020

Keywords:
Local surface plasma resonance (LSPR)
Ag/Al_2O_3 ordered array
Damping resonance
Refractive index

ABSTRACT

In this study, an ordered metal oxide-metal composite system was designed. By changing the thickness of film of Ag/Al_2O_3 nanoparticles (NPs), the red and blue shifts of local surface plasma resonance (LSPR) were realized in the proposed system and discussed by damping resonance theory and Mie's scattering theory to demonstrating the relationship between wavelength (λ) and particle diameter (D). With the increasing of sputtering time of Ag, the SPR of Ag was red shifted under the influence of damped vibration, obtaining that square of wavelength (λ^2) is proportional to D. The surface plasma resonance (SPR) of Ag/Al_2O_3 showed an obvious blue shift, and then red shift suddenly, which is affected by the competition between damping resonance and refractive index. When the blue shift occurs, the change of wavelength ($\Delta\lambda$) is exponentially related to the diameter (D). The modulation of LSPR of the proposed composite nano-metal materials will have a potential application in SPR sensor and surface enhanced Raman scattering (SERS).

1. Introduction

With the development of science and technology, human's understanding of nature has achieved a leap from macro to micro. Under the influence of surface effect, small size effect, quantum size effect, macroscopic quantum tunneling effect and dielectric confinement effect, nano-metal materials have achieved special optical properties mainly due to the surface plasma resonance (SPR), which attracts people's attention [1]. In recent years, the SPR has played an important role in many fields, such as light capture, photocatalysis, surface enhanced Raman scattering (SERS) and surface enhanced fluorescence, especially in the field of sensors [2]. LSPR is very sensitive to the size, shape, and environmental conditions of nanoparticles (NPs). The blue shift or red shift of LSPR can be adjusted by changing the size and shape of LSPR in a fixed surrounding medium. People have been keen on the regulation of LSPR. Compared with the modulation of red shift, the modulation of blue shift is more concerned, but the modulation of blue shift and red shift appears simultaneously is rarely realized. Adjustable LSPRs are widely used in energy transfer applications, solar cells and so on, among which the recent application of very hot biosensors is the most noticeable [1,3,4].

Noble metals (such as Au, Ag and Cu) have become the best plasma materials due to controllable of SPR [5–8]. The three materials have their own advantages and disadvantages. Au NPs have excellent biocompatibility and are not easy to oxidize, but they are expensive. Cu NPs are cheap, but are limited by extreme instability. Under the same conditions, the LSPR effect of silver nanostructures is generally better than that of Au and Cu nano-structures [6,8]. Because of the toxicity and oxidization of Ag, we choose to build a coating on the surface of NPs [8–10]. The growing interests in alumina oxide (Al_2O_3) are related to their unique advantages such as high specific surface area, excellent pore structure, thermal stability and low price [11]. Furthermore, Al_2O_3 as a coating not only can remove physically adsorbed water and chemically adsorbed hydrides, but also prevent oxidation and surface passivation. It has been used in structural electrodes, surface-enhanced Raman scattering, catalysis and sensing fields [9,12–17]. So it is a good choice to cover the surface of Ag with Al_2O_3.

However, the effect of Al_2O_3 on the SPR of Ag cannot be neglected. As we all know, the SPR of Ag is in the visible region, but that of metal oxide is in the infrared region. Metal oxides have some influence on the optical properties of nanocrystalline plasma, the most obvious manifestation is the shift of the ultraviolet LSPR. In recent years, LSPRs have been studied by changing the size, shape, dielectric properties of noble metals and core-shell composition of NPs, achieving a blue shift or red shift, but few of them have both red shift and blue shift in the system [18–21]. Bharat Tandon et al. used electrochemical potential to

* Corresponding authors.
E-mail addresses: jhyang1@jlnu.edu.cn (J. Yang), chenlei@jlnu.edu.cn (L. Chen).

https://doi.org/10.1016/j.saa.2020.118430
1386-1425/

modulate metal oxide-doped nano-system [19]. The experiment is too difficult and the process is complex. It is an effective method to modulate metal oxide-metal composite system by simple layer-by-layer sputtering to achieve blue shift and red shift simultaneously and to explore the interaction between blue shift and red shift in the same system [22–24].

Here, single-layer ordered arrays by using the hydrophilicity of single-layer colloidal spheres was fabricated. The ordered PS/Ag/Al_2O_3 arrays on the basis of single-layer colloidal spheres by simple magnetron sputtering technology. On the one hand, the single-layer ordered array achieves the uniformity of structural materials. on the other hand, it avoids the coupling effect between layers. Moreover, the structure of nanospheres can effectively increase the optical path, concentrate energy and improve the utilization of light. In PS/Ag/Al_2O_3 ordered array system, with the increase of Ag sputtering time, the diameter of the spheres is also increasing, which leads to the movement of LSPR. The PS/Ag/Al_2O_3 ordered array can adjust the absorbance in the field of ultraviolet-visible-infrared. The expansion of the light absorption range will not only be of great value in the field of battery, SPR sensor and SERS, but also provide a new direction for the development of new nano-metal materials [25–27].

2. Experimental section

2.1. Chemicals and materials

Silicon (Si) wafer (100) was purchased from Hefei Kejing Material Technology Co., Ltd. Ag and Al_2O_3 with 99.99% purity were purchased from Beijing Tianrui Science and Technology Development Center. Monodisperse polystyrene (PS) colloidal particles with a size of 200 nm (10 wt.% aqueous solution) were purchased from Thermo Fisher Limited company. Ethanol (analytical reagent) was purchased from China Chemical Plant. Sodium dodecyl sulfate (SDS, analytical reagent), H_2O_2 (30%) and NH_4OH (25%) were all purchased from National Pharmaceutical Chemical Reagent Co., Ltd. They were the highest purity available and the chemical reagents use without further purified. Deionized ultrapure water (18.25 MΩ cm^{-1}) and silicon (Si) wafers were used throughout the present study.

2.2. Characterization

Morphology and microstructure images of the Ag/Al_2O_3 arrays were obtained using a JEOL 6500F scanning electron microscope (SEM) and a JEM-2100HR transmission electron microscopy (TEM) respectively, operating at an accelerating voltage of 200 kV. Ultraviolet-visible (UV–Vis) absorption spectra were obtained using a Shimadzu UV-3600 spectrometer.

2.3. Preparation of glass and hydrophilic silicon wafers

A large piece of silicon wafer was immersed in 10% SDS aqueous solution for 24 h to make its surface hydrophilia. The sizes of silicon and glass wafers were 2.0 cm×2.0 cm and 2.0 cm×1.0 cm separately. The wafers were heated to 300°C in the mixed solution of NH_4OH and H_2O_2. After cooling, the wafers were cleaned with ethanol and ultrapure water in turn, and then put into ultrapure water for use.

2.4. Preparation of the ordered PS arrays

The prepared PS template and anhydrous ethanol were mixed in a ratio of 1:1 to form a mixed solution. After ultrasonic treatment, the mixed solution was evenly dripped onto the hydrophilic silicon wafers surface, and then the silicon wafer was slowly inserted into the water, which made the mixed solution float off the silicon wafer and formed a tightly arranged single-layer array structure. The prepared small silicon wafers (size 2.0 cm×2.0 cm) and glass wafers (size 2.0 cm×1.0 cm) were dipped into the array obliquely and lifted. After drying, the ordered arrays existed on silicon or glass wafers. Such silicon or glass wafers were used for magnetron sputtering substrates.

2.5. Fabrication of multilayered Ag/Al_2O_3 arrays on PS template

The Ag/Al_2O_3 ordered arrays on the PS template were fabricated by a magnetron sputtering system (ATC 1800-F, USA AJA). Ag was sputtered at 10 W for 0, 30, 60, 90, 120 and 180 s, respectively, while Al_2O_3 was sputtered for 3 min at 100 W with a working pressure of 6.0×10^{-1} Pa. Fig. 1 shows the schematic of the fabrication process of PS/Ag/Al_2O_3 ordered arrays [22,28–32]. First, PS ordered array was prepared. After that, Ag was sputtered with the same power and different sputtering time on the PS array. Then, Al_2O_3 was sputtered with the same time and power. Finally, PS/Ag/Al_2O_3 ordered array was obtained. In the Fig. 1, green is PS colloid sphere, yellow is Ag, and the purple part is Al_2O_3.

2.6. Result and discussion

As we all know, the morphology of the substrate is one of the most important parameters affecting the properties of materials, and the SEM is the most common method to describe the basic morphology. Figs. 2 and 3 are the SEM images of Ag and Al_2O_3 layered sputtering with the same sputtering power and different sputtering time for 0, 30, 60, 90, 120 and 180 s. As shown in Fig. 2, with the increasing of the sputtering time for Ag, the particles on the surface of the sphere are more and more obvious, and the diameter of the sphere is also increasing. There is a distinct sense of granularity in the SEM images from Fig. 2a to f, which is most evident in Fig. 2f. The diameter of nanocrystalline increases with the increase of sputtering time. The diameter of nanocrystalline with sputtering time of 120–180 s increases obviously, which is shown in Fig. 2e-f and Fig. 3e-f. The charging trends of diameter of nanocrystalline are consistent with film thicknesses measured by the step profiler. According to the step profiler, film thicknesses are 14, 20, 24, 33, 50 and 52 nm respectively. And the diameter of PS sphere is 200 nm. Therefore, the semi-shell structure with different thicknesses of the Ag/Al_2O_3 covers on the surface of PS sphere. The change of the color between samples can be clearly seen through optical pictures: PS/Al_2O_3 (a) is light purple. With the increase of the Ag content, the color gradually changes to dark purple in the Fig. 2c-e. Even the color turns yellow-green in the Fig. 2f. Fig. 3 can well verify the discovery of Fig. 2, which is that the diameter of the sphere is proportional to the sputtering time. There is a certain relationship between the color change of the samples and the diameter of the spheres, mainly due to the binding effect of the refractive index, which will be explained in detail later.

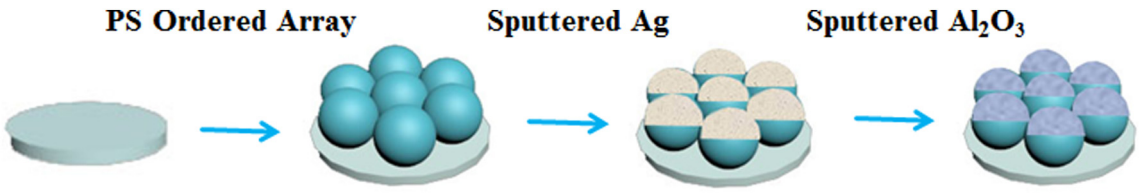

Fig. 1. The schematic of the fabrication process for PS/Ag/Al_2O_3 ordered arrays.

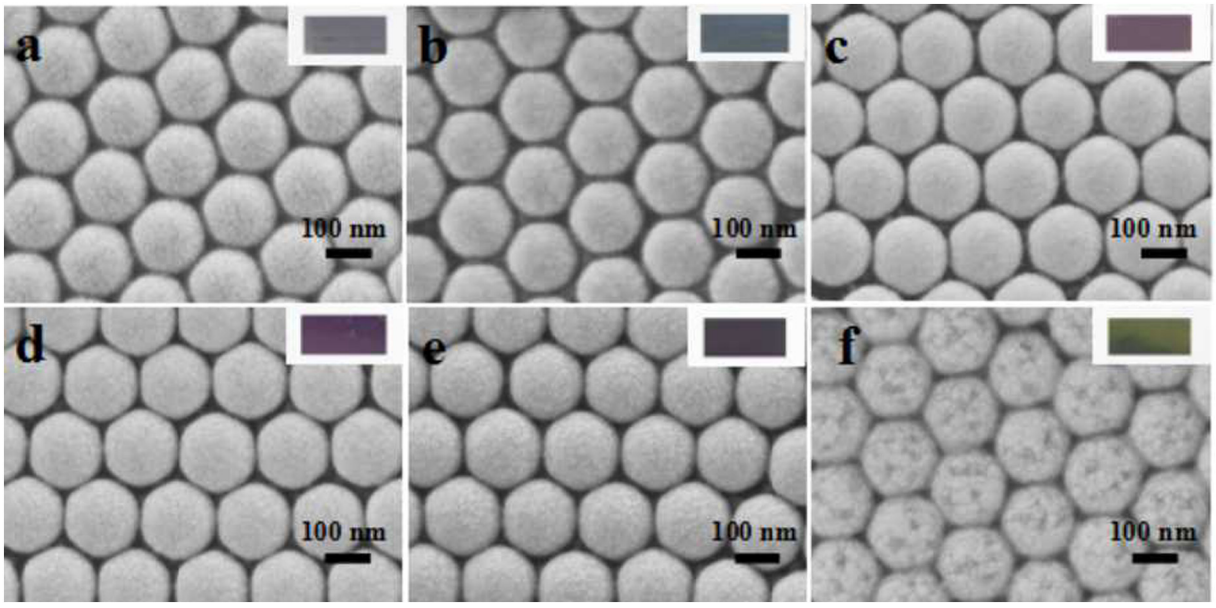

Fig. 2. SEM images of Ag/Al_2O_3 ordered array consisting of Ag with constant sputtering power (10 W) at different sputtering time and Al_2O_3 with the same sputtering power (100 W) at the same sputtering time (3 min) .The sputtering time of Ag is (a) 0, (b) 30, (c) 60, (d) 90, (e) 120, (f) 180 s. (The illustrations are the corresponding optical photographs separately.)

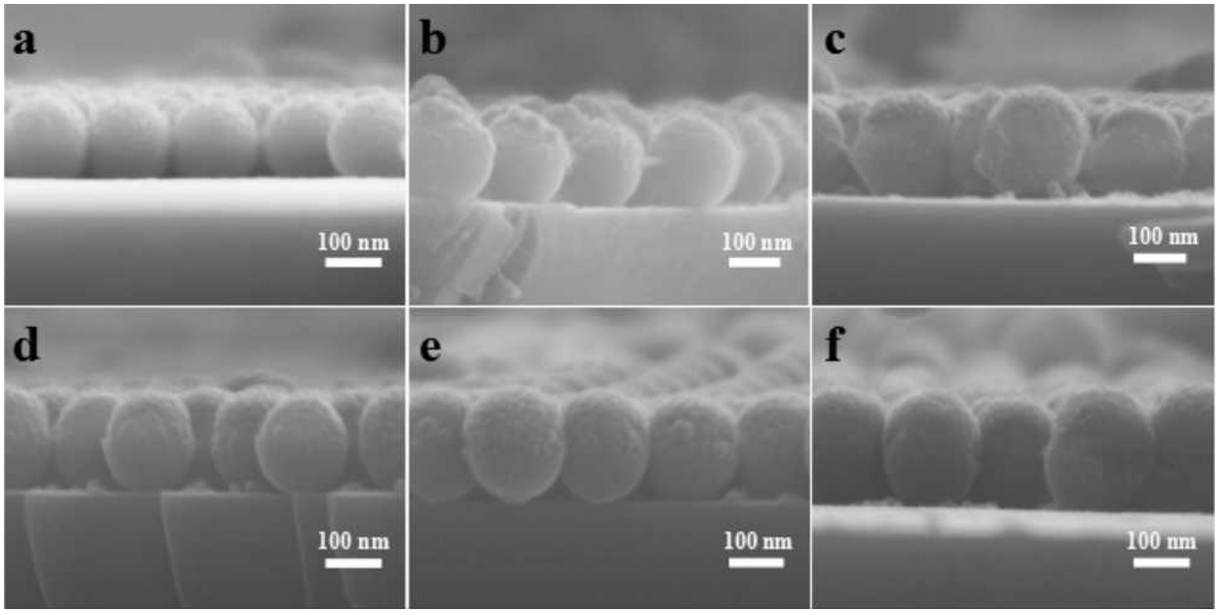

Fig. 3. The cross section SEM images of Ag/Al_2O_3 ordered array composed of Ag/Al_2O_3 with constant sputtering power (10 W) at different sputtering time and same sputtering power (100 W) at the same sputtering time (3 min).The sputtering time of Ag is (a) 0, (b) 30, (c) 60, (d) 90, (e) 120 and (f) 180 s.

In addition, the detailed morphology and microstructures of the as-obtained PS/Al_2O_3 and PS/Ag (120 s)/Al_2O_3 samples were investigated by TEM showed in Fig. 4. As illustrated in Fig. 4a, TEM images of PS/Al_2O_3 and PS/Ag/Al_2O_3 exhibited a characteristic shape with the diameter of about 210 and 250 nm, which correspond to the SEM images. As depicted in Fig. 4b, Al_2O_3 shown in HR-TEM is noncrystal under the condition of sputtering power of 100 W and sputtering time of 3 min. Furthermore, the TEM and HR-TEM images of PS/Ag/Al_2O_3 composite were also employed. As displayed in Fig. 4d, a lattice spacing observed of 0.2077 nm is in good agreement with the crystal plane of Ag (110), indicating the formation of PS/Ag/Al_2O_3 composites. Fig. 4e-g are the element distribution diagram of Ag and Al respectively. However, in Fig. 4g, it is found that the range of Al is slightly more than that of Ag, which is consistent with layer-by-layer sputtering. It also shows that Al_2O_3 is sputtered on the outside of Ag.

As we all know, the increase of the diameter of the sphere has a great influence on the absorption of light. Fig. 5 is the UV–Vis absorbance spectra of Ag. Fig. 6 is the UV–Vis absorbance spectra of layer-by-layer sputtering of PS/Ag/Al_2O_3, pure PS and pure Al_2O_3. In Fig. 5 and Fig. 6, the sputtering power for Ag and Al_2O_3 are 10 and 100 W. The sputtering time for Al_2O_3 is keep constant (3 min) and for Ag are 30, 60, 90, 120 and 180 s, respectively. With the increase of sputtering time for Ag, the redshift of the SPR is due to the influence of dielectric constant in the Fig. 5. However, with the Al_2O_3 sputtering time and power unchanged, the Ag sputtering time increased, the SPR of PS/Ag/Al_2O_3 at about 1000 nm blue-shifted and then red-shifted, and at about 400 nm showed a slight redshift. This phenomenon is quite different from that of Ag deposited on the PS arrays and is worth studying. In order to better describe the change of the absorption position, the peak position of the plasma resonance peak of PS/Ag/Al_2O_3 was shown in Table.1. Combining of Fig. 6

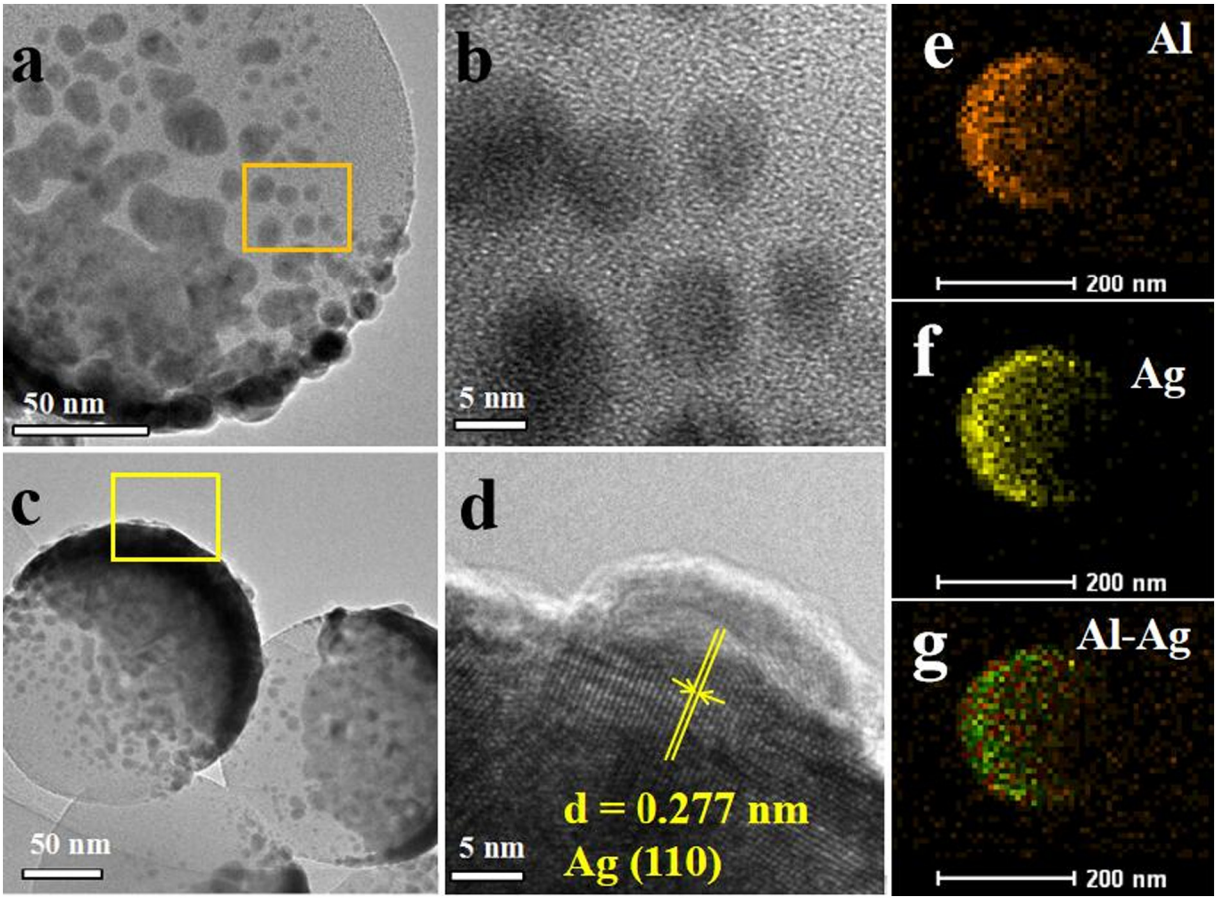

Fig. 4. TEM images: TEM and HR-TEM images of pure Al_2O_3(a, b); TEM and HR-TEM images of Ag/Al_2O_3 with Ag (c, d), EDX mapping of Ag/Al_2O_3 (e-g). (The sputtering time of Ag is 120 s).

and Table 1, we can find that the peaks of about 300 nm (peak 1) and about 520 nm (peak 3) are basically unchanged with the increase of Ag content. Peak at 522 nm is the plasma resonance peaks of Al_2O_3 and peak at about 299 nm is belong to PS sphere, because the content of Al_2O_3 and PS between NPs is unchanged. The attribution of peak position is also verified in the UV spectra of pure PS and pure Al_2O_3, though the SPR shifts due to the change of carrier concentration. When the sputtering time of Ag increases to 180 s, there is a slight shift of peak at 522 nm, which is mainly due to the influence of the coupling of Ag and Al_2O_3. However, two peaks at 331 and 1289 nm are changed obviously. Peaks at 331 and 1289 nm are attributed to the LSPR of Ag and PS/Ag/Al_2O_3, From the variation of peak 2 in Fig. 6 and Table 1, we can

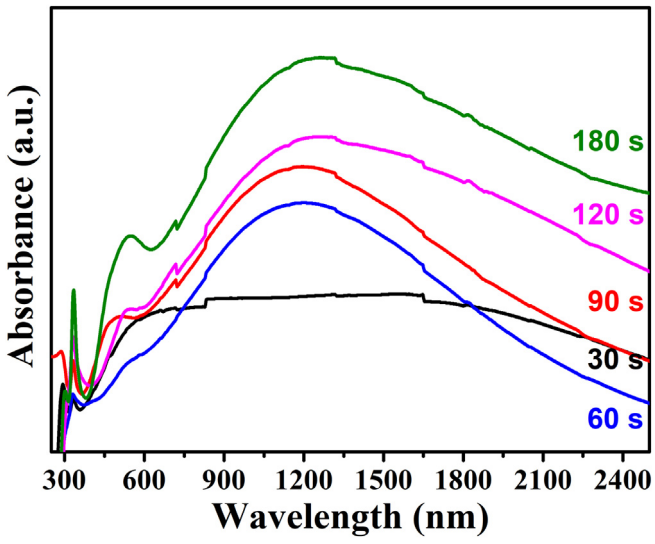

Fig. 5. UV–Vis absorption spectra of Ag with constant sputtering power (10 W) and different sputtering time (30, 60, 90, 120 and 180 s) deposited on PS arrays.

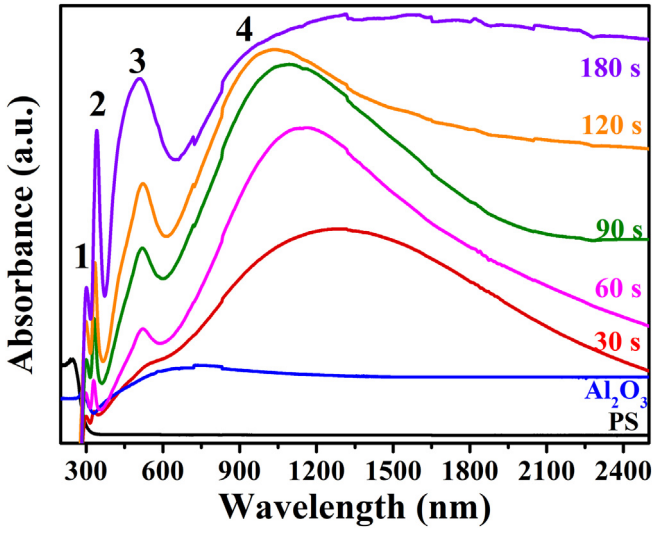

Fig. 6. UV–Vis absorption spectra of Ag with constant sputtering power (10 W) and different sputtering time (30, 60, 90, 120 and 180 s) and Al_2O_3 with constant sputtering power (100 W) and sputtering time (3 min) deposited on PS arrays by layer-by-layer sputtering and of pure PS arrays and of pure Al_2O_3 with constant sputtering power (100 W) and sputtering time (3 min).

Table 1
Peak position of UV–Vis absorption spectra of Ag and Al_2O_3 with constant sputtering power (10 W) and different sputtering time (30, 60, 90, 120 and 180 s) and constant sputtering power (100 W) and sputtering time (3 min) deposited on PS arrays by layer-by-layer sputtering.

	Wavelength (nm)					Peak position change	Attribution problem
	30 s	60 s	90 s	120 s	180 s		
1	299	299	299	299	299	No change	PS
2	331	329	331	333	341	Blue shift red shifts	Ag
3	522	522	522	522	507	No change	Al_2O_3
4	1289	1163	1093	1036	1314	Blue shift red shifts	PS/Ag/Al_2O_3

see that the LSPR of Ag shows an indistinct blue shift firstly and then red shift obviously. The LSPR of PS/Ag/Al_2O_3 shows an obvious blue shift, and then a sudden red shift. In order to better understand the reason of peak change, we divide it into two parts: Ag and PS/Ag/Al_2O_3 for in-depth analysis.

2.7. Analysis of SPR of Ag by damping resonance theory

In order to understand the reasons of variation of the LSPR, the theory of damped resonance was employed to explain the red shift of the absorption peak of Ag. Taking the original Al_2O_3 as the raw material, Ag sputtered at different time is equivalent to adding different resistance to hinder the resonance phenomenon. According to the Newton's second law of classical theory,

$$M\frac{d^2x}{dt^2} + kx(t) = -F(t) \tag{1}$$

Here $F(t)$ is the resistance, which is proportional to the sputtering time. $\frac{d^2x}{dt^2}$ is the acceleration of simple harmonic motion, and the restoring force of $kx(t)$ is proportional to the distance from the original position of vibration.

Based on Laplacian transformation, $L(f^{(n)}) = P^nL(f) - P^{n-1}f(0) - \ldots - f^{(n-1)}(0)$;

obtain,

$$L\left(\frac{d^2x}{dt^2}\right) = P^2L(x) \tag{2}$$

Replace formula 2 with formula 1, which is expressed as

$$mP^2L(x) + kL(x) = F(x) \tag{3}$$

According to the transfer function, $G(x) = \frac{L(x)}{F(x)} = \frac{1}{mP^2 + k}$.

From the general form of the second order system $\omega = \sqrt{\frac{k}{m}}$, k is a constant and m is the total mass. Accordingly, $c = \lambda \times \omega, \lambda = c/\sqrt{\frac{m}{k}}, \lambda^2 = \frac{c^2}{k}m$. Then, λ^2 is proportional to m. During the sputtering process, the mass increases with the time of sputtering Ag, so λ^2 is proportional to the sputtering time. According to SEM and the step profiler, λ^2 is proportional to the particle diameter (D).

In order to verify this conclusion, we simulate the curve of the relationship between time and the square of the wavelength. Fig. 7 is the variation curve of the square of the wavelength and mass. It is obvious that the red shift occurs between 60 and 180 s, which completely agree well with the theory of damped resonance. However, the blue shift occurs within 30–60 s, which is inconsistent with the theoretical calculation. This is mainly due to the fact that the resonance phenomenon is not obvious when the Ag content is very low. Our conclusions coincide with those obtained by coupling theory.

In coupling theory, long-range dipole coupling leads to the blue shift of LSPR, while red shift is due to near-field coupling between many nanometer dimers or small aggregates of NPs [33]. Near-field coupling obeys the plasma rule equation proposed by El-Sayed and co-workers. The ratio of resonance wavelength shift $\Delta\lambda$ to monomer resonance wavelength λ_0 follows an exponential dependence on the ratio of inter-particle separation d to particle diameter D given by.

$$\Delta\lambda/\lambda_0 = Ae^{-(d/D)/\tau} + B \tag{4}$$

where $\Delta\lambda$ denotes the resonance wavelength shift with respect to the monomer resonance wavelength λ_0, τ is the decay constant, which is roughly 0.2, and A and B are two constants [34]. The simulated absorption spectrum of plasma and the corresponding regular equation of plasma are fitted as shown in Fig. 8. The agreement between SPR of Ag and the formula not only explains the red shift of SPR of Ag, but also holds in the PS/Ag/Al_2O_3 system.

Through the change of peak 2 in Fig. 6 and Table 1, we have deeply explored the change of SPR, and obtained the relationship between the change of SPR position and sputtering time of Ag. With the increase of sputtering time, the change of wavelength increases gradually. This means that the phenomenon of damped vibration is more obvious.

2.8. Analysis of SPR of PS/Ag/Al_2O_3 by refractive index

With the increasing of the sputtering time for Ag from 30 to 120 s, the SPR of Ag/Al_2O_3 was an obvious blue shift, which is mainly due to the effect of the refractive index [19]. Mie's scattering theory reveals the relationship between refractive index and particle diameter. Further, Mie resonances, with the advantage of ultrastrong light-matter interaction in micrometer-scale particle, are sensitive to the particle's dimensions and geometry [35–38]. Based on the simple Drude model, metals are treated as free electron gases, and the relationship between wavelength and refractive index is as follows:

$$\lambda_{sp} = \lambda_p\sqrt[2]{1 + K_1n_1^2} \tag{7}$$

where λ_{sp} represents the wavelength of SPR, λ_p represents the wavelength of peak, K_1 represents geometry factor, n_1 is the refractive index of the surrounding effective material [39]. In the formula, the wavelength of the SPR is proportional to the refractive index. It is also

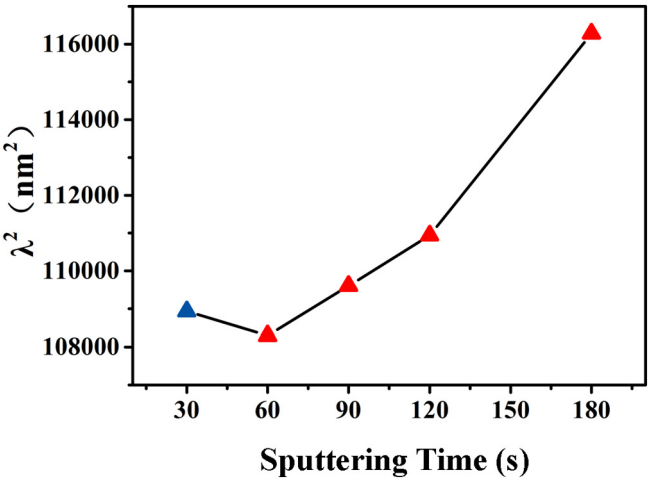

Fig. 7. Variation curve of square of SPR of Ag with sputtering time of Ag and particle diameter (D).

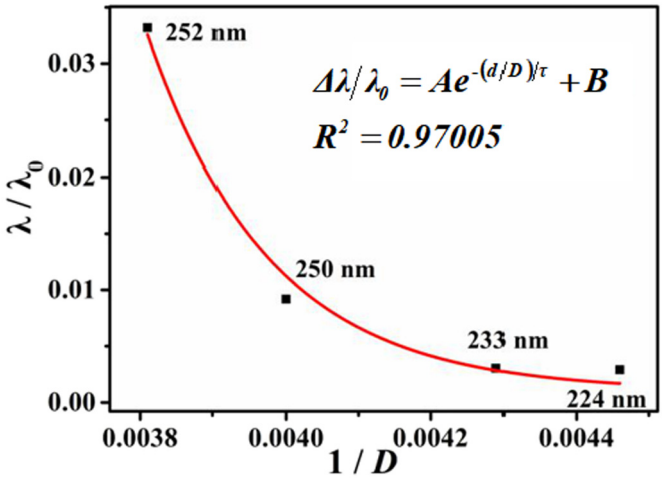

Fig. 8. The relationship between plasma displacement and particle diameter.

proved that the increase of particle diameter leads to the decrease of the refractive index, which eventually leads to the blue shift of the SPR.

Moreover, the decrease of effective ambient refractive index leads to the increase of relative refractive index, which further leads to the change of color from light purple to yellow-green, which is also consistent with the blue shift of wavelength.

2.9. Competition between damping resonance and refractive index

Fig. 9 shows the changes in the global LSPR. The whole SPR resonance band is mainly affected by two factors: refractive index and damping resonance. According to SEM and the step profiler, the increase of the Ag particle diameter between 30 and 120 s causes the change of refractive index. The influence of refractive index on LSPR is greater than damping resonance, which leads to blue shift. When the sputtering time is 180 s ($D = 252$ nm), the whole SPR appears a red shift. This red shift can be assigned to the increased charge separation during plasma oscillation by the increase in size. The charge separation leads to the lattice distortion and lengthen chemical bond, resulting in the decrease of the SPR intrinsic vibration frequency of NPs and the SPR moving to higher wavelength. It is found that the damping resonance is more and more obvious through the SPR of Ag, leading to the dominant position of damping resonance station when the sputtering time is 180 s. There may be an equilibrium position between 120 and 180 s to make the refractive index equal to the effect of damping resonance.

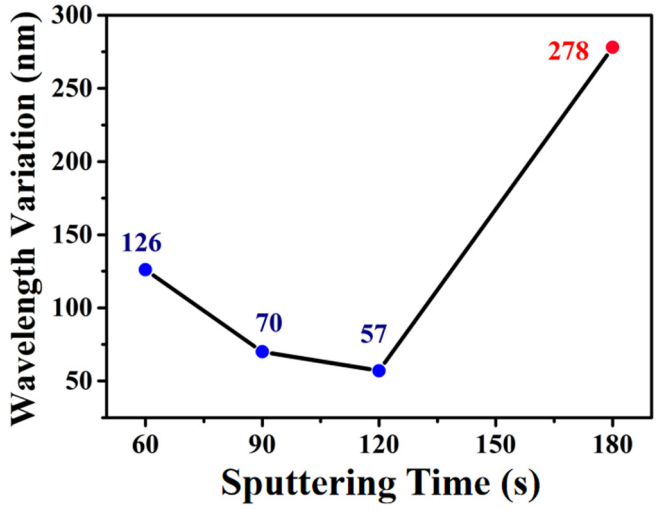

Fig. 9. Fractal charts of wavelength variation and sputtering time of the SPR of Ag/Al_2O_3.

3. Conclusions

In summary, we have successfully prepared Ag/Al_2O_3 ordered array on PS template through layer-by-layer sputtering technology, and controlled the size of NPs by adjusting the sputtering time, so as to realize the modulation of LSPR. With the increase of NPs, the LSPR of Ag shows a significant red shift in the UV region, which is mainly caused by the damping resonance. For the SPR of Ag, the square of the wavelength (λ^2) is proportional to the particle diameter (D), and the variation of the wavelength ($\Delta\lambda$) is in accordance with the plasma rule equation proposed by El-Sayed and co-workers. In the Ag/Al_2O_3 ordered array, the collective LSPR is affected by the competition of refractive index and damping resonance, and there is a sudden red shift after the obvious blue shift. The blue shift between 30 and 120 s is due to the increase of refractive index and wavelength (λ) is proportional to refractive index, which is greater than the damping resonance. This red shift can be assigned to the increased charge separation during damping resonance by the increase in size. When sputtering time is 180 s, the diameter is too large and the damping resonance causes a red shift. This kind of composite can change the modulation of LSPR by particle size. Al_2O_3 covered on Ag surface avoids the oxidation, thereby prolongs the life of sensing material. The influence of refractive index on LSPR has also been proved, which will provide a basis for refractive index sensing. In addition, the modulation effect of LSPR broadens the application in the UV–visible-infrared region.

CRediT authorship contribution statement

Daxin Zhang: Conceptualization, Data curation, Formal analysis, Investigation, Methodology, Writing - original draft, Writing - review & editing. **Shuo Yang:** Investigation, Formal analysis. **Xin-Yuan Zhang:** Conceptualization, Methodology, Formal analysis. **Ning Ma:** Investigation, Methodology. **Bingbing Han:** Investigation, Methodology. **Wenshi Zhao:** Investigation. **Shaohua Chi:** Investigation. **Yang Liu:** Funding acquisition, Project administration. **Jinghai Yang:** Conceptualization, Funding acquisition, Project administration, Supervision. **Lei Chen:** Conceptualization, Formal analysis, Funding acquisition, Project administration, Supervision, Writing - review & editing.

Declaration of competing interest

The authors declare that they have no known competing financial interests or personal relationships that could have appeared to influence the work reported in this paper.

Acknowledgments

This work was supported by the National Natural Science Foundation of China (grant nos. 61775081 and 21676115), the National Key Research and Development Program of China (grant no. 2017YFF0108607), Program for the Development of Science and Technology of Jilin province (item no. 20180519016JH), the National Youth Foundation of China (grant no. 51609100) and Project of Jilin Development and Reform Commission (2019C051-3).

References

[1] P. Bhatia, S.S. Verma, M.M. Sinha, Phys. Lett. A 383 (2019) 2542–2550.
[2] L. Chen, Y. Zhao, Y. Wang, Y. Zhang, Y. Liu, X.X. Han, B. Zhao, J. Yang, Analyst 141 (2016) 4782–4788.
[3] N. Gordillo, S. Catalan-Gomez, L. Pau, A. Redondo-Cubero, Nanotechnology 30 (2019) 1–10.
[4] L.P.F. Peixoto, J.F.L. Santos, G.F.S. Andrade, Anal. Chim. Acta 1084 (2019) 71–77.
[5] J. Zhu, X. Li, J.J. Li, J.W. Zhao, Spectrochim. Acta A 189 (2018) 571–577.

[6] Z. Shang, M. Wang, S. Pan, X. Sun, G. Shi, X. Yan, W. Ma, T. Jiao, Opt. Commun. 451 (2019) 345–352.
[7] J.F. Li, Y.F. Huang, Y. Ding, Z.L. Yang, S.B. Li, X.S. Zhou, F.R. Fan, W. Zhang, Z.Y. Zhou, D.Y. Wu, B. Ren, Z.L. Wang, Z.Q. Tian, Nature 464 (2010) 392–395.
[8] B.M. Kim, M.S.P. Reddy, Y.W. Lee, C. Park, Opt. Commun. 450 (2019) 276–281.
[9] T. Ikuno, J. Zheng, A. Vjunov, M. Sanchez-Sanchez, M.A. Ortuno, D.R. Pahls, J.L. Fulton, D.M. Camaioni, Z.Y. Li, D. Ray, B.L. Mehdi, N.D. Browning, O.K. Farha, J.T. Hupp, C.J. Cramer, L. Gagliardi, J.A. Lercher, J. Am. Chem. Soc. 139 (2017) 10294–10301.
[10] L.J. Cui, S. Hur, Z.A. Akbar, J.C. Klockner, W. Jeong, F. Pauly, S.Y. Jang, P. Reddy, E. Meyhofer, Nature 572 (2019) 628–634.
[11] N. Ma, L. Chen, T. Jing, X.Y. Zhang, B.B. Han, X.X. Xue, Y.J. Zhang, B. Zhao, J. Phys. Chem. C 123 (2019) 28846–28851.
[12] J. Ephraim, D. Lanigan, C. Staller, D.J. Milliron, Chem. Mater. 28 (2016) 5549–5553.
[13] C.M. Staller, Z.L. Robinson, A. Agrawal, S.L. Gibbs, B.L. Greenberg, S.D. Lounis, U.R. Kortshagen, D.J. Milliron, Nano Lett. 18 (2018) 2870–2878.
[14] Y. Liu, Z. Xu, M. Yin, H. Fan, W. Cheng, L. Lu, Y. Song, J. Ma, X. Zhu, Nanoscale Res. Lett. 10 (2015) 374.
[15] M.D. Alonso-Murias, J.S. Velazquez-Gonzalez, D. Monzon-Hernandez, J. Lightwave Technol. 37 (2019) 4808–4814.
[16] T. Wang, M.J. Zhang, K. Liu, J.F. Jiang, Y.H. Zhao, J.Y. Ma, T.G. Liu, Opt. Commun. 448 (2019) 93–97.
[17] A.K. Sharma, J. Gupta, IEEE Sensors J. 19 (2019) 8775–8780.
[18] D. Song, D. Jing, J. Colloid. Interf. Sci. 505 (2017) 373–382.
[19] B. Tandon, A. Agrawal, S. Heo, D.J. Milliron, Nano Lett. 19 (2019) 2012–2019.
[20] Y.C. Pu, G.M. Wang, K.D. Chang, Y.C. Ling, Y.K. Lin, B.C. Fitzmorris, C.M. Liu, X.H. Lu, Y.X. Tong, J.Z. Zhang, Y.J. Hsu, Y. Li, Nano Lett. 13 (2013) 3817–3823.
[21] D.W. Vogt, A.H. Jones, H.G.L. Schwefel, R. Leonhardt, Opt. Lett. 44 (2019) 1319–1322.
[22] N. Ma, X.Y. Zhang, W. Fan, S. Guo, Y. Zhang, Y. Liu, L. Chen, Y.M. Jung, Spectrochim. Acta A 219 (2019) 147–153.
[23] X.Y. Zhang, D. Han, N. Ma, R. Gao, A. Zhu, S. Guo, Y. Zhang, Y. Wang, J. Yang, L. Chen, J. Phys. Chem. Lett. 9 (2018) 6047–6051.
[24] X.-Y. Zhang, D. Han, Z. Pang, Y. Sun, Y. Wang, Y. Zhang, J. Yang, L. Chen, The J. Phys. Chem. C 122 (2018) 5599–5605.
[25] X. Zhang, X.S. Zhu, Y.W. Shi, Opt. Lett. 44 (2019) 4550–4553.
[26] L.Y. Niu, Q. Wang, J.Y. Jing, W.M. Zhao, Opt. Commun. 450 (2019) 287–295.
[27] J. Zhou, J.S. Zhang, H.T. Yang, Z. Wang, J.A. Shi, W. Zhou, N. Jiang, G.Y. Xian, Q. Qi, Y.X. Weng, C.M. Shen, Z.H. Cheng, S.T. He, Nanoscale 11 (2019) 11782–11788.
[28] X.-M. Li, M.-H. Bi, L. Cui, Y.-Z. Zhou, X.-W. Du, S.-Z. Qiao, J. Yang, Adv. Funct. Mater. 27 (2017) 1–9.
[29] Y. Wang, L. Li, G. Li, Appl. Surf. Sci. 393 (2017) 159–167.
[30] Y. Wang, X. Zhao, L. Chen, S. Chen, M. Wei, M. Gao, Y. Zhao, C. Wang, X. Qu, Y. Zhang, J. Yang, Langmuir 30 (2014) 15285–15291.
[31] Y. Wang, X. Zhao, W. Gao, L. Chen, S. Chen, M. Wei, M. Gao, C. Wang, Y. Zhang, J. Yang, RSC Adv. 5 (2015) 7454–7460.
[32] X.-Y. Zhang, L. Chen, Y. Wang, Y. Zhang, J. Yang, H.C. Choi, Y.M. Jung, Spectrochim. Acta A 197 (2018) 37–42.
[33] J.A. Jenkins, Y.D. Zhou, S. Thota, X.D. Tian, X.W. Zhao, S.L. Zau, J. Zhao, J. Phys. Chem. C 118 (2014) 26276–26283.
[34] P.K. Jain, W. Huang, M.A. El-Sayed, Nano Lett. 7 (2007) 2080–2088.
[35] W. Ji, L. Li, W. Song, X. Wang, B. Zhao, Y. Ozaki, Angew. Chem. Int. Ed. Engl. 58 (2019) 14452–14456.
[36] K.E. Klug, C.M. Jennings, N. Lytal, L. An, J.-Y. Yoon, Roy. Soc. Open Sci. 6 (2019) 1–12.
[37] M. Khutia, G.M. Joshi, K. Deshmukh, M. Pandey, Polym.-Plast. Technol. 54 (2015) 383–389.
[38] K.R. Berry, R.L. Romo, M. Mitchell, V. Bejugam, D.K. Roper, J. Nanomater. 2019 (2019) 1–11.
[39] W. Chen, H. Hu, W. Jiang, Y. Xu, S. Zhang, H. Xu, Chinese Phys. B 27 (2018) 1–21.